

## Relative depletion of niobium in some arc magmas and the continental crust: partitioning of K, Nb, La and Ce during melt/rock reaction in the upper mantle

Peter B. Kelemen<sup>a</sup>, Nobumichi Shimizu<sup>a</sup>, Todd Dunn<sup>b</sup>

<sup>a</sup> Department of Geology and Geophysics, Woods Hole Oceanographic Institution, Woods Hole, MA 02543, USA

<sup>b</sup> Department of Geology, University of New Brunswick, Fredericton, N.B. E3B 5A3, Canada

(Received April 1, 1993; revised and accepted October 13, 1993)

---

### Abstract

Depletion of Nb relative to K and La is characteristic of lavas in subduction-related magmatic arcs, as distinct from mid-ocean ridge basalts. Nb depletion is also characteristic of the continental crust. This and other geochemical similarities between the continental crust and high-Mg# andesite magmas found in arcs suggests that the continental crust may have formed by accretion of andesites. Previous studies have shown that the major element characteristics of high-Mg# andesites may be produced by melt/rock reaction in the upper mantle. In this paper, new data on partitioning of K, Nb, La and Ce between garnet, orthopyroxene and clinopyroxene in mantle xenoliths, and on partitioning of Nb and La between orthopyroxene and liquid, show that garnet and orthopyroxene have Nb crystal/liquid distribution coefficients which are much larger than those of K and La. Similar fractionations of Nb from K and La are expected in spinel and olivine. For this reason, reactions between migrating melt and large masses of mantle peridotite can produce substantial depletion of Nb in derivative liquids. Modeling shows that reaction between ascending, mantle-derived melts and mantle peridotite is a viable mechanism for producing the trace element characteristics of high-Mg# andesite magmas and the continental crust.

Alternatively, small-degree melts of metabasalt and/or metasediment in the subducting slab may leave rutile in their residue, and will thus have large Nb depletions relative to K and La [1]. Slab melts are too rich in light rare earth elements and other incompatible elements, and too poor in compatible elements, to be parental to arc magmas. However, ascending slab melts may be modified by reaction with the mantle. Our new data permit modeling of the trace element effects of reaction between small-degree melts of the slab and mantle peridotite. Modeling shows that this type of reaction is also a viable mechanism for producing the trace element characteristics of high-Mg# andesites and the continental crust. These findings, in combination with previous results, suggest that melt/rock reaction in the upper mantle has been an important process in forming the continental crust and mantle lithosphere.

---

[CH]

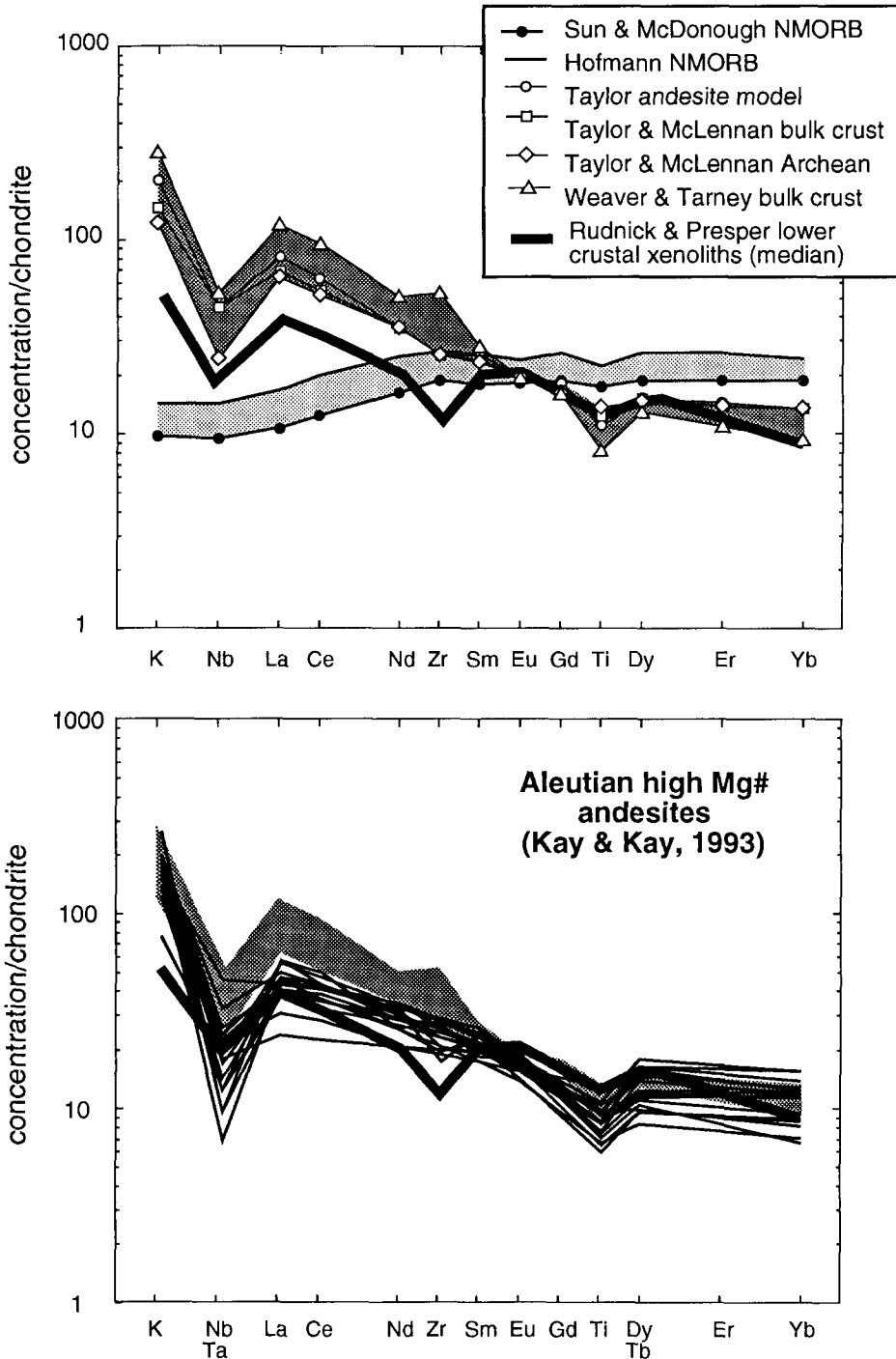


Fig. 1. Trace element composition for estimated average compositions of continental crust [4,5], the median composition of lower crustal xenoliths [7], high Mg# andesites from the intra-oceanic, Aleutian magmatic arc [8] and normal mid-ocean ridge basalts [6,9], plotted in approximate order of increasing abundance in normal MORB. Both estimated average compositions for the continental crust, and the median composition of xenoliths from the lower continental crust, are light REE enriched, have heavy REE and Ti lower than MORB, and have depletions of Nb and Ti relative to neighbor elements on this compatibility diagram. In the lower plot, the hachured region illustrates the estimated composition of the bulk continental crust, and the bold line is the median composition for lower crustal xenoliths. The high-Mg# andesites, while slightly lower in total REE concentration than the

## 1. Introduction: high-Mg# andesites and the continental crust

In this paper we develop trace element models in support of the hypothesis that many magmas in subduction-related magmatic arcs are modified by reaction between ascending melts and surrounding mantle peridotites. Some of these magmas have 55–65 wt% SiO<sub>2</sub> and a percentage (by weight) of MgO/(MgO + FeO<sub>14</sub>) greater than 0.35. These, referred to as high-Mg# andesites, are similar in both major and trace element characteristics to the continental crust. Thus, we propose that continental crust may have formed as a result of accretion of high-Mg# andesites. A second paper will discuss the major element characteristics and genesis of high-Mg# andesites and the continental crust. The Mg#, Ni content and Cr content of high-Mg# andesites are too high for them to have formed by crystal fractionation and/or melting from basaltic source compositions. Instead, experimental and theoretical investigations have shown that they can be produced by reaction between ascending liquids and mantle peridotite. Other processes, such as magma mixing and assimilation of crustal, granitic rocks in basaltic magmas, have demonstrably formed high-Mg# andesites in specific cases and may have played a role in the genesis of the crust. However, crustal mixing processes cannot produce andesitic crust if the net flux through the Moho is basaltic.

We have not attempted to model the origin of all arc basalts and andesites, although they have many similarities. We have concentrated on high-Mg# andesites because their composition is so nearly identical to that of the continental crust.

We infer that this similarity is not a coincidence and indicates the operation of similar processes in their formation. High-Mg# andesites are less abundant than basaltic lavas among volcanic rocks in contemporary island arcs. This observation has led to the hypothesis that arc crust formed at present is basaltic. If the continental crust formed by direct accretion of mantle-derived, andesitic magmas in arcs, then either arc magmatism must have changed character with time, or andesites may be more abundant in specific tectonic environments, or andesitic parts of arc crust are selectively preserved to form continental crust, or the hypothesis that crustal composition in contemporary arcs is basaltic is incorrect, and the middle to lower arc crust is andesitic. These possibilities are explored in the second paper in this series.

In the initial section of this paper, we present new data on partitioning of K, Nb, La, Ce and other elements between minerals in mantle peridotite and between orthopyroxene and basaltic liquid. These partition coefficients are then used to model fractionation of Nb from K and La in a variety of melting and melt/rock reaction processes, in order to explain depletions of Nb relative to K and La found in magmas in subduction-related magmatic arcs. Depletion of Nb and Ta relative to highly incompatible, “large ion lithophile” elements (LILE), such as Ba, Th, K, as well as to the light rare earth elements (REE) La and Ce, is characteristic of arc magmas, and is not observed in mid-ocean ridge basalts [e.g., 2,3]. Nb depletion relative to K and La is also characteristic of the continental crust [4,5]. Since La/Nb in mid-ocean ridge basalt (MORB) is generally less than or equal to chondritic values, and K, La,

---

bulk crust, have La/Yb similar to crustal values and REE abundances similar to those in lower crustal xenoliths. The andesites and continental crust share very similar depletions of Nb and Ta from K and La, and of Ti from Gd, Tb and Dy. In addition, although this is not illustrated here, high-Mg# andesites and continental crust have similar concentrations of other crucial petrogenetic indicators, such as Ni, Cr, Rb and Sr. In this and all subsequent trace element diagrams, all concentrations have been normalized to those in C1 chondrites [69] except for K, for which 9 times the reported concentration is divided by the chondritic abundance. The 17 andesite and basaltic andesite compositions were chosen from the data base of Aleutian volcanic rock compositions compiled by Kay and Kay [8]; they comprise all the data for lavas from the intra-oceanic portion of the Aleutian arc with reported Ta and La concentration, wt% SiO<sub>2</sub> between 54 and 63 (average 58.5), and wt% MgO/(MgO + FeO<sub>14</sub>) from 0.29 to 0.54 (average 0.38). The lavas selected come from more than ten separate volcanic centers, most of them on different islands. For the andesite compositions, chondrite-normalized concentrations of Ta and Tb are plotted in place of Nb and Dy, respectively; Nb and Dy concentrations are plotted for all other compositions.

and Nb vary systematically in MORB [e.g., 6], it is thought that these elements are not strongly fractionated by melting of spinel lherzolite. Thus, Nb is generally plotted between K and La on extended rare earth, or “compatibility”, diagrams.

In Fig. 1, we present a compatibility diagram with estimates of the trace element composition of the continental crust [4,5,7], and high-Mg# andesites from the intra-oceanic, Aleutian arc [8], compared to normal MORB [6,9]. In general, continental crust and high-Mg# andesites are enriched in incompatible elements, showing a smooth negative slope on the diagram. As in many other arc magmas, Nb depletion relative to K and La in high-Mg# andesites and in the continental crust is accompanied by a depletion of Ti relative to the middle rare earth elements Eu, Tb and Dy. There may also be a depletion of Zr relative to Nd and Sm in the continental crust and in some arc magmas. This feature is potentially obscured in crustal estimates, since they rely heavily on the composition of detrital sediments and upper crustal crystalline rocks with a sedimentary component, which are likely to be enriched in zircon by weathering.

## 2. Origin of high field strength element depletions in arc magmas

Saunders et al. [10] termed Nb and Ta, together with Zr, Hf, Ti and V, as “high field strength elements” (HFSE). There are numerous theories for the origin of HFSE depletions in arc magmas, but no consensus. One hypothesis is that Nb and Ta are relatively insoluble in hydrous fluids evolved by the dehydration of the downgoing slab in a subduction zone, compared to LILE and light REE [e.g., 10,11]. Metasomatism by these fluids may enrich the mantle source of arc magmas in LILE and light REE, but not Nb and Ta. The charge/radius ratio of monatomic ions is positively correlated with solubility in some aqueous fluids, as deduced from the relative “mobility” of elements during hydrothermal alteration of mafic volcanic rocks [e.g., 2], and as observed in experiments [12] which showed that Nb is less mobile than LILE and REE during dehydration

of serpentine at 12 kbar and 850°C. More recently, however, Ayers and Watson [13] demonstrated that rutile ( $\text{TiO}_2$ ) solubility in fluids is pressure dependent, increasing by 3 orders of magnitude from 10 to 30 kbar. Thus, experiments at 10–15 kbar may not be directly relevant to fluids generated beneath arcs. At 30 kbar rutile is nearly 100 times more soluble than LILE- and REE-rich monazite, so that fluids saturated in minor phases within a subducting slab may be enriched in Ti, Zr and other HFSE relative to the LILE and LREE, not depleted.

A related hypothesis is that reaction between migrating hydrous fluids and peridotite may fractionate HFSE from LILE and REE, producing metasomatized mantle in the source for arc magmas. Olivine/fluid partition coefficients for some incompatible elements, but none of the HFSE, have been measured in saline  $\text{H}_2\text{O}$ – $\text{CO}_2$  fluids by Brennan and Watson [14]. Hawkesworth et al. [11] showed that these partition coefficients vary systematically with monatomic ionic radii. Extending this relationship to the HFSE, they illustrated that fluid/peridotite reaction could reproduce the relative abundance pattern for incompatible elements in arc magmas. However, they showed that the Brennan and Watson solid/liquid partition coefficients are two to three orders of magnitude too large to account for the absolute abundance of incompatible elements in arc magmas. In addition, Randle and Odling [15] found that fluids in equilibrium with hydrated, partially molten peridotite show no fractionation of Nb from La and K. In summary, recent results cast some doubt upon the hypothesis that aqueous fluid metasomatism creates relative Nb and Ta depletions in the source of arc magmas.

Related to the aqueous fluid metasomatism hypothesis is the theory that high  $f_{\text{H}_2\text{O}}$  and/or  $f_{\text{O}_2}$  in the subducting slab or the mantle wedge stabilizes HFSE-rich trace phases, resulting in HFSE depletions in co-existing fluids and/or melts [e.g., 16]. However, relatively high concentrations of Ti and Zr are needed for saturation of basaltic magmas in rutile and zircon. Since such high concentrations are unusual, particularly in mafic arc magmas, the presence of Ti- and/or Zr-rich accessory phases is unlikely in the resid-

ual source of mafic arc magmas. Thus, HFSE depletions probably do not result from equilibria between mafic magmas and accessory phases in the mantle [1].

HFSE depletions may result from equilibria between silicic magmas and rutile. Rutile is stable on the liquidus for silicic magmas generated by partial melting of hydrous basaltic rocks at pressures exceeding 15–20 kbar [1,17,18]. Residual rutile is present at temperatures as high as 1150°C, with melt fractions exceeding 25 wt% at 32 kbar [18]. Experimentally observed Nb rutile/liquid distribution coefficients for basaltic liquids are in the range of 16–30, or more [19,20], so partial melts of basalt in equilibrium with rutile, garnet and clinopyroxene will commonly be depleted in Nb and enriched in LREE and LILE. Ryerson and Watson [1] proposed that HFSE anomalies in arc magmas arise by mixing of a slab-derived, siliceous partial melt of hydrous metabasalt with depleted peridotite.

Alternatively, HFSE depletions may result from reaction between ascending basaltic liquids and depleted peridotite in the mantle wedge [21,22]. Previous studies showed that mantle orthopyroxene, olivine and spinel all have higher crystal/liquid distribution coefficients for Ti and Zr than they do for neighbor REE on a compatibility diagram [21–25], and thus can create Ti and Zr depletions. We designed this study to investigate the possibility of similar behaviour for Nb relative to K and La.

### 3. Previous measurements of Nb distribution

Prior data on partitioning of Nb between rock-forming minerals in mantle peridotite, and between minerals and melt, are fairly few and far between. More measurements have been made on clinopyroxene (Cpx) than on any other phase. Our preferred value,  $D_{\text{Nb}}^{\text{Cpx/liq}} = 0.0077$ , comes from Hart and Dunn [26], who used the ion probe to analyze 24 trace elements at natural abundance levels on a Cpx/alkali basalt pair equilibrated at 30 kbar. Green et al. [27] report an Nb distribution coefficient for garnet and basaltic liquid of 0.02. However, garnets were strongly

zoned in Nb, with a core to rim variation of 121–47 ppm in one experiment. Nonetheless, our data (below) confirm their value for  $D_{\text{Nb}}^{\text{garnet/liq}}$  to within a factor of two. R. Nielsen and co-workers [pers. commun., 1993] have measured Nb partitioning between magnetite, Al–Cr spinels and doped basaltic liquids. In general,  $D_{\text{Nb}}^{\text{spinel/liq}}$  varies regularly with  $D_{\text{Ti}}^{\text{spinel/liq}}$ , such that  $D_{\text{Nb}} = D_{\text{Ti}}/15$ . In keeping with this relationship, Nielsen et al. measured  $D_{\text{Nb}}^{\text{spinel/liq}}$  of approximately 0.01 for spinel–chromite solid solutions crystallized from primitive, high-Mg# basaltic liquid. Pearce and Norry [28] summarize phenocryst/matrix partitioning data for Nb in kaersutite, biotite, magnetite, orthopyroxene (Opx), clinopyroxene and plagioclase, mainly from volcanic rocks with 60–70 wt% SiO<sub>2</sub>. Their extrapolation yields reasonable values for basaltic magmas and suggests that Nb is as compatible in Opx as in co-existing Cpx.

## 4. Analytical methods used in this study

### 4.1. Ion probe procedure for all samples

Relative trace element abundance was determined by secondary ion mass spectrometry using the Cameca IMS 3f ion microprobe at the Woods Hole Oceanographic Institution. A primary beam of negative oxygen ions with a current of about 4 nA was focused to a spot 30–50 μm in diameter. Positive secondary ions were analyzed by a double focusing mass spectrometer; energy filtering to reduce molecular interference [29] involved a high-energy offset of –105 eV and a bandpass of ±25 eV for a net secondary accelerating voltage of 4370–4420 eV. Under these conditions, the isotope abundance corrected count rate for Si in clinopyroxene standard KH1 is about 6 million counts/sec. After 5 min of preliminary sputtering, secondary beam intensities were measured in five cycles; counting <sup>39</sup>K, <sup>47</sup>Ti, <sup>52</sup>Cr, <sup>90</sup>Zr, <sup>93</sup>Nb, <sup>139</sup>La and/or <sup>140</sup>Ce for 30 s each, and <sup>23</sup>Na and <sup>30</sup>Si for 5 s. Intensities for other elements are reported relative to Si to reduce the effect of variation of the primary beam current. At the present time, there are no mineral standards at Woods Hole for Nb and K in mantle phases. Two

phase partition coefficients are calculated directly from these ion intensity ratios, corrected for the relative abundance of Si in each phase.

We verified that intensities are related to Nb concentration at the ppm level, using natural glass samples 972-1, 975-1, D6-23 and D7-8A, originally analyzed by Bender et al. [30] and KL-2 analyzed by Jochum [31, and pers. commun., 1989]. Intensity/concentration results are illustrated in Fig. 2a. Some variation in the intensity/concentration ratio may be due to analytical error in glass compositions determined by XRF, or to heterogeneity in the glasses. Based on these data and prior experience with the ion microprobe, we are confident that there is a linear relationship between ion intensity and Nb concentration at these abundance levels.

#### 4.2. Preparation and analysis of experimental charges

Partitioning between Opx and basaltic liquid was determined in two experimental charges doped with Nb and La at the percent level. The starting material was a synthetic, high-Mg# andesitic melt. Fusion and crystallization experiments were at 1 atm, with oxygen fugacities along the fayalite–magnetite–quartz buffer, imposed with CO–CO<sub>2</sub> gas mixtures. The initial mix was decarbonated and then fused twice, for 2 h each time, at 1380°C. After each fusion, it was crushed by grinding in an agate mortar under acetone. Splits of the powders were doped with reagent grade La<sub>2</sub>O<sub>3</sub> and Nb<sub>2</sub>O<sub>5</sub>, homogenized by grinding under acetone, and then fused for 1 h at 1380°C. Liquidus temperatures for each mixture were experimentally determined. In synthesis experiments, the sample was fused for 1 h at 1380°C, rapidly cooled over 6 min to 1245°C, to grow crystal nuclei, heated at 1°C/h to 1260°C, and then held at that temperature for 57.5 h. Under these conditions the mixtures crystallized small amounts (< 20 volume%) of olivine and Opx. Samples were quenched in distilled water. The major element composition of the charges, determined via electron microprobe, is reported in Table 1. Ion microprobe analysis of Opx was complicated by the skeletal shape of the crystals.

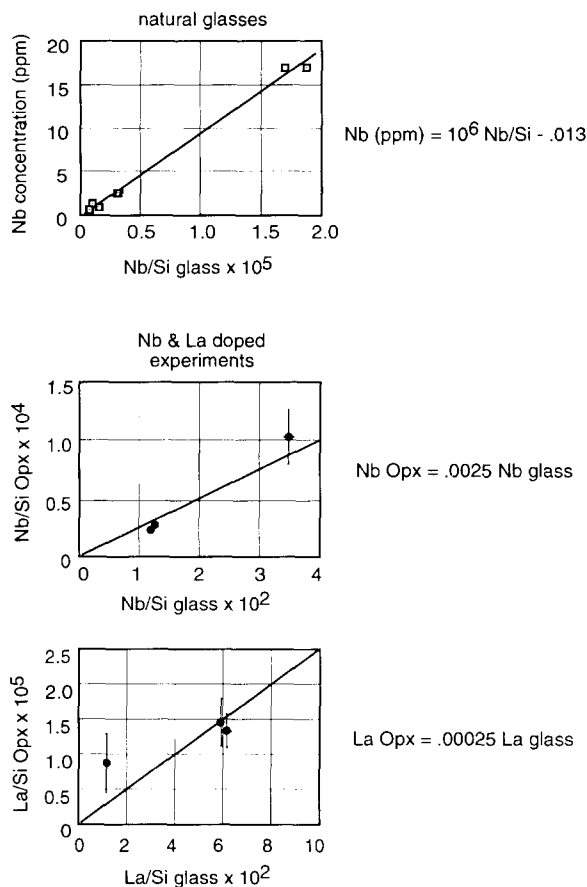


Fig. 2. Ion microprobe analyses of natural glasses and of experimental orthopyroxene/basaltic glass pairs doped with Nb and La, synthesized at 1 bar. In this and subsequent illustrations of ion probe results, ion intensity ratios observed by mass spectrometry are corrected for isotopic abundance and then reported as ratios to the total Si intensity. The top diagram illustrates the intensity/concentration relationship for basaltic glasses with other reported analyses of Nb concentration. Si intensity is measured at <sup>30</sup>Si and corrected for isotopic abundance. The bottom two diagrams show the ion intensities for Nb and La in orthopyroxene and coexisting glass. Points are sample averages, collected for two samples on two different days. Error bars are for 1 s.d. See text and Tables 1 and 2a for further information.

Secondary ions are produced outside the optically observable "crater" produced by the focused ion beam. Measured Nb and La intensities in Opx showed considerable variation to higher values, with a plateau of lower values (reported in Table 2 and Figs. 2b and c) comprising data obtained from larger crystals. We interpret higher values

Table 1

Major element composition of phases in experimental charges analyzed by ion probe in this study

Values in weight percent. Glass, olivine, and orthopyroxene compositions in experimental charges determined by microprobe analysis at the University of New Brunswick, with a JEOL JSM 6400 electron microscope equipped with a Link eXL energy dispersive analyzer and a single wavelength dispersive spectrometer, with an accelerating voltage of 15 keV and a sample current of 2.5 nA on the Faraday cup. Na was analyzed by WDS, while the other elements were analyzed simultaneously by EDS. The ferrous iron content of the starting glasses were determined via redox titration and Fe<sub>2</sub>O<sub>3</sub> was determined by the difference between the wet chemical and electron probe determinations of FeO and FeO\*. Bulk compositions are nominal weights used in oxide mixtures. See text for experimental conditions and Table 2A for ion probe results

run phase	66A bulk	66A glass	66A olivine	66A opx	66B bulk	66B glass	66B olivine	66B opx
SiO <sub>2</sub>	53.95	53.27	40.30	56.24	53.30	53.44	40.64	56.73
TiO <sub>2</sub>	.25	.31			.24	.12		
Al <sub>2</sub> O <sub>3</sub>	12.62	12.79		.89	12.47	12.53		1.03
Fe <sub>2</sub> O <sub>3</sub>	1.06				5.82			
FeO*	6.15	6.73	10.39	5.86	1.33	6.27	9.56	5.83
MnO	.17			.20	.17		.10	.19
MgO	12.00	10.19	48.34	34.59	11.85	10.03	49.40	34.70
CaO	6.49	6.47	.08	.36	6.41	6.63	.19	.31
Na <sub>2</sub> O	1.90	2.06			1.88	2.26		
K <sub>2</sub> O	.70	.66			.69	.59		
P <sub>2</sub> O <sub>5</sub>	.07				.07			
La <sub>2</sub> O <sub>3</sub>	1.01	1.02			4.64	4.92		
Nb <sub>2</sub> O <sub>5</sub>	3.96	3.98			1.28	1.12		
	100.33	97.48	99.11	98.14	100.15	97.91	99.89	98.79

\* All Fe as FeO in EDS analyses of glass, olivine and orthopyroxene. FeO in bulk composition determined by titration. Fe<sub>2</sub>O<sub>3</sub> by difference from total Fe content.

Table 2a

Results of ion probe analyses of glass and orthopyroxene in doped experimental charges. Major element analyses of coexisting phases reported in Table 1

	n	Ti/Si	st dev	V/Si	st dev	Cr/Si	st dev	Zr/Si	st dev	Nb/Si	st dev	La/Si	st dev
9/9/92 avg Opx 66A	4	.000666	60	.000014	2	.000882	55	.000004	1	.000103	23	.000009	4
9/9/92 avg glass 66A	3	.004671	200	.000031	2	.000249	10	.000184	15	.034798	822	.011603	547
9/9/92 Opx/glass 66A		.143		0.46		3.54		.023		.0030		.00075	
9/9/92 avg Opx 66B	3	.000762	132	.000017	1	.001013	135	.000005	1	.000027	3	.000013	2
9/9/92 avg glass 66B	3	.005669	360	.000041	3	.000274	8	.000236	21	.012633	151	.061446	2021
9/9/92 Opx/glass 66B		.134		0.41		3.69		.022		.0022		.00022	
2/4/92 avg Opx 66A	5							.000005	1	.000159 *	21	.000041	13 *
2/4/92 avg glass 66A	2							.000240	5	.034757	1117	.011431	75
2/4/92 Opx/glass 66A								.019		.0046 *		.00361	*
2/4/92 avg Opx 66B	2							.000004	1	.000023	3	.000015	3
2/4/92 glass 66B	1							.000246	4	.011908	86	.059006	206
2/4/92 Opx/glass 66B								.015		.0019		.00025	
avg Opx/glass		.139		0.43		3.62		.02		.002		.0004	

\* Values in italics apparently include glass contamination in Opx analyses. They are not included in average Opx/glass values and are not plotted in Fig. 2.

Table 2b

Results of ion probe analyses of coexisting phases in garnet peridotite xenoliths. Major element analyses of coexisting phases reported in Table 1.

	n	K/Si	st dev	Zr/Si	st dev	Nb/Si	st dev	La/Si	st dev	Ca/Si	st dev	
clinopyroxene (Cpx)												
FRB 348	4	.000132	9	.00002300	171	.00000062	9	.000005440	943	.000023600	4750	
JJG 348	2	.000415	113	.00001040	0.1	.00000069	3	.000006680	403	.000022800	707	
PHN 1925	2	.000277	9	.00002670	57	.00000038	0.1	.000002190	106	.000006840	375	
AJE 25	6	.000508	(n=1)	.00003250	83	.00000032	10	.000001580	121	.000007750	595	
garnet												
FRB 348	5	.000008	*	9	.00015261	759	.00000083	8	.000000067	31	.000000823	83
JJG 348	5				.00009200	1140	.00000116	7	.000000147	53	.000001160	118
PHN 1925	2	.000016	*	13	.00014819	45	.00000081	3	.000000091	7	.000000597	16
AJE 25	7				.00024874	1070	.00000044	8	.000000050	8	.000000539	33
orthopyroxene (Opx)												
FRB 348	2	.000005	*	(n=1)	.00000053	4	.00000024	0.1	.000000013	3	.000000087	5
JJG 348	2				.00000046	5	.00000024	4	.000000037	3	.000000104	9
PHN 1925	2	.000021	*	13	.00000182	4	.00000010	1	.000000031	3	.000000160	3
AJE 25	2	.000027	*	8	.00000089	12	.00000014	5	.000000023	4	.000000082	34
Cpx/liquid [ref. 59]		.0072		.1234		.0077		.0536		.0858		
garnet/Cpx												
FRB 348		<0.063		6.6		1.3		.012		.035		
JJG 348				8.8		1.7		.022		.051		
PHN 1925		<0.056		5.6		2.2		.041		.087		
AJE 25				7.7		1.4		.032		.070		
average		<0.060	.005	7.2	1.4	1.6	0.4	.027	.013	.061	.023	
garnet/liquid **												
		<0.0003		0.7		.01		.001		.004		
Opx/Cpx												
FRB 348		<0.036		.023		.39		.002		.004		
JJG 348				.044		.35		.006		.005		
PHN 1925		<0.076		.068		.26		.014		.023		
AJE 25		<0.054		.027		.46		.014		.011		
average		<0.055	.020	.041	.020	.36	.08	.009	.006	.011	.009	
Opx/liquid **												
		<0.0004		.006		.003		.0005		.001		

\* K/Si values for garnet and orthopyroxene are maxima and may include substantial Na + O interference at mass 39. Therefore garnet/clinopyroxene and orthopyroxene/clinopyroxene values are reported as maxima. See text for further discussion.

\*\* Crystal/liquid distribution coefficients in this table calculated on the basis of coexisting phase compositions reported here, modified using Si garnet/Si Cpx of 0.8 and Si Opx/Si Cpx of 1.1, combined with Cpx/liquid distribution coefficients from Hart and Dunn [26].

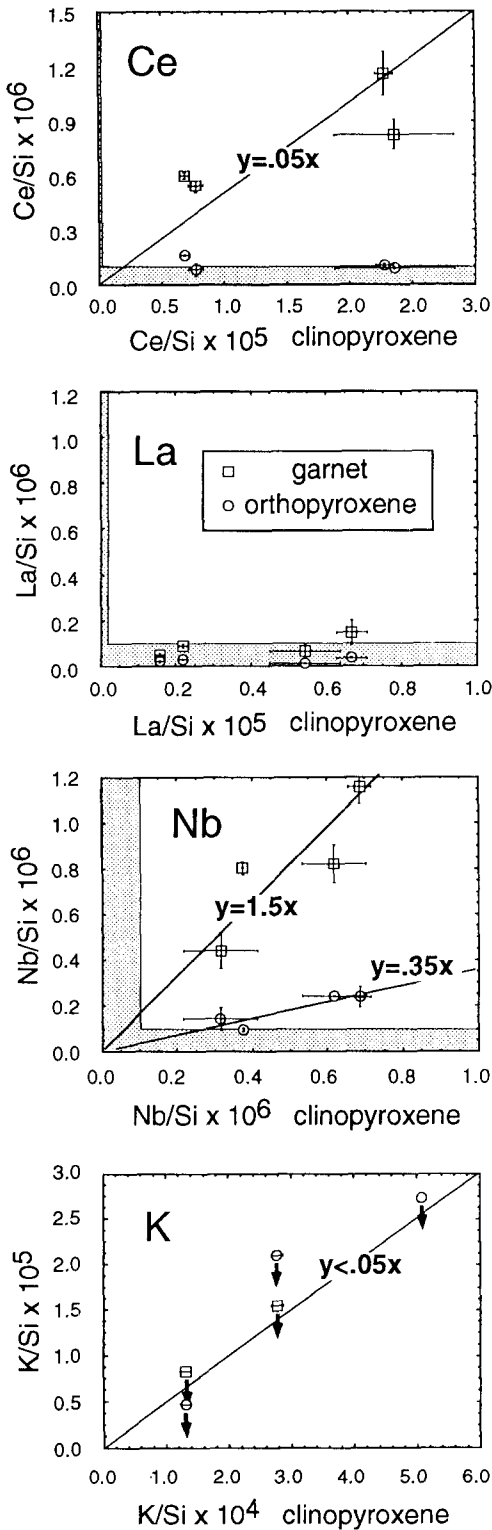
as including Nb and La counts from small glass inclusions and/or glass excited by primary beam scatter, and plateau values as analyses obtained purely from Opx.

#### 4.3. Trace element analyses of co-existing minerals in garnet lherzolite samples

Partitioning between garnet, Opx and Cpx was determined in four garnet lherzolite xenoliths from South African kimberlites. Whole rock and mineral analyses for two of these samples, AJE 25 and PHN 1925, have been previously published [32,33]. Richardson et al. [34] showed that

garnet and Cpx in AJE 25 were in Nd isotopic equilibrium. Major element data for other samples are available from the authors upon request. Results of our ion probe analyses are reported in Table 2 and Fig. 3. Both cores and "rims" of relatively large crystals were analyzed, but the outer 50  $\mu\text{m}$  of each crystal were avoided, since prior studies have shown substantial zoning in the outermost rim of crystals in otherwise well equilibrated garnet lherzolite xenoliths.

Count rate ratios for  $^{39}\text{K}/^{30}\text{Si}$  in garnet and Opx showed substantial time dependence, decreasing by a factor of more than five during a 15 min analysis. This is unlike  $^{39}\text{K}/^{30}\text{Si}$  in Cpx in the



same samples, and unlike <sup>93</sup>Nb/<sup>30</sup>Si, <sup>139</sup>La/<sup>30</sup>Si and <sup>140</sup>Ce/<sup>30</sup>Si in all three phases, which were nearly constant. The time dependence of “<sup>39</sup>K”/<sup>30</sup>Si in garnet and Opx may be due to initially high production of <sup>23</sup>Na<sup>16</sup>O<sup>-</sup>, a molecular interference at mass 39. We have used only the final K/Si ratio (fifth of five) from each analysis block in calculating K/Si in garnet and Opx. The data appear surprisingly systematic (Fig. 3), but reported K partition coefficients for garnet/Cpx, garnet/liquid, Opx/Cpx and Opx/liquid must be considered maximum values.

### 5. Analytical results

Table 2 and Fig. 3 present analytical results. Variation in the mineral/mineral partitioning data between samples exceeds the standard deviation in the measurements for a single sample. This may be indicative of disequilibrium, or of equilibration under different conditions of temperature, pressure, and/or bulk composition. In addition, there are problems with analytical uncertainty in analyzing the natural samples. As can be seen in Fig. 3, our measurements for La and Ce in Opx, and for La in garnet, are close to our estimated detection limits for these elements. Partitioning values based on these measurements should be considered maxima.

Despite these caveats, there are many consistent results in these data. Garnet/Cpx ratios for La are less than 0.05, Opx/Cpx ratios for La are less than 0.02. The ratio of Nb in garnet/Cpx

Fig. 3. Ion microprobe analyses of coexisting phases in four garnet lherzolite samples from the Kapvaal Craton, southern Africa. Square symbols are sample averages for garnet/Cpx and circles are for Opx/Cpx. Error bars are for 1 s.d. from the mean. Hatched area along the x and y axes illustrates maximum estimated analytical blank, based on ion intensities measured on olivine in undoped experimental charges. In the bottom diagram, for K partitioning results, plotted values are considered maxima because of time dependent decreases in the <sup>39</sup>K/<sup>30</sup>Si intensity ratio in garnet and Opx during the analyses, probably due to mass interference by <sup>23</sup>Na<sup>16</sup>O<sup>-</sup>. See text and Table 2b for further information.

ranges from 1.3 to 2.2, and Nb in Opx/Cpx ranges from 0.26 to 0.43. Thus, most importantly, analytically determined distribution coefficients for Nb are *at least ten times larger* than distribution coefficients for La and K in Opx/Cpx and garnet/Cpx in all samples analyzed. This is true despite the fact that the relative abundances of K and La in Opx and garnet are maximum estimates. Mineral/mineral partitioning data were combined with the Cpx/basaltic liquid partitioning data of Hart and Dunn [26] to produce the

calculated mineral/basaltic liquid partition coefficients presented in Table 2b. The values calculated for Nb and La in Opx/liquid, 0.003 and 0.0005, are the same, within analytical uncertainty, as values of 0.002 and 0.0004 obtained directly from Opx/glass analyses of the experimental charges (Table 2a).

Table 3 and Fig. 4 illustrate a set of compiled trace element crystal/liquid distribution coefficients for basalt to basaltic andesite compositions in equilibrium with mantle phases. Most are com-

Table 3

Crystal liquid distribution coefficients for mantle phases in equilibrium with basaltic magmas in the upper mantle, except for rutile/liquid, which is for partial melts of basaltic compositions at high pressure

element	D olivine/liq	ref	D Opx/liq	ref	D Cpx/liq	ref	D spinel/liq	ref	D garnet/liq	ref	D rutile/liq	ref
K	.000000001	1	.00001	1,3	.0072	6	0	1	.00001	1,3	0	1
Nb	.0001	1	.003	3	.0077	6	.01	7	.01	3	30	11
La	.000007	1,2	.0005	3	.0536	6	.0006	8	.001	3	0	1
Ce	.00001	2	.0009	3	.0858	6	.0006	8	.004	3	0	1
Nd	.00007	2	0.009	4,5	.1873	6	.0006	8	0.057	4,10	0	1
Zr	.0005	2	.014	3,4,5*	.1234	6	.07	1,9	0.3	3,4,10**	40	1
Sm	.0007	2	.02	4,5	.291	6	.0006	8	0.5	4,10	0	1
Eu	.00095	1,2	.03	4,5	.350	6	.0006	8	1	4,10	0	1
Gd	.0012	2	.04	4,5	.400	6	.0006	8	2	4,10	0	1
Ti	.015	2	.14	4,5	.384	6	.15	7,9	0.6	4,10	-	12
Dy	.004	2	.06	4,5	.442	6	.0015	8	2.5	4,10	0	1
Er	.009	2	.07	4,5	.387	6	.003	8	3	4,10	0	1
Yb	.023	2	.1	4,5	.430	6	.0045	8	4	4,10	0	1

## References

- 1 Interpolated value. In the case of Nb in olivine, value is based on known fractionation of Zr and Ti from neighboring elements on compatibility diagrams.
  - 2 McKay [36], and Kelemen and McKay unpublished ion probe results on experimental olivine/glass pairs.
  - 3 This paper. Ion probe results on experimental Opx/glass pairs and on coexisting phases in mantle peridotites.
  - 4 Shimizu et al., unpublished ion probe results on coexisting phases in mantle peridotites.
  - 5 Dick and Kelemen [23] ion probe on Opx/Cpx pairs in Trinity and Josephine mantle peridotites.
  - 6 Hart and Dunn [26] ion probe results on 30 kbar experimental Cpx/glass pair.
  - 7 R. Nielsen [pers. commun. 1993], based on long counting time WDS electron probe analyses of doped experimental charges. See text.
  - 8 Stosch [42] INM analyses of coexisting phases in spinel peridotite xenoliths.
  - 9 Kelemen et al. [21] mainly based on WDS electron probe analyses of 10 kbar experimental charges of Kinzler and Grove [70].
  - 10 Salters [35], ion probe results on coexisting phases in garnet peridotite xenoliths.
  - 11 Green and Pearson [20] WDS electron probe analyses of coexisting rutile and Nb doped andesitic glass.
  - 12 Ryerson and Watson [1], showed that the Ti content of liquid coexisting with rutile cannot be described using crystal/liquid distribution coefficients.
- \*  $D(\text{Zr})$  Opx/liquid used here is less than that determined from experimental Opx/glass pairs in this study. Note that there is a large discrepancy between the Opx/glass value (Table 2a) and the one determined based on coexisting phase compositions in garnet lherzolite xenoliths (Table 2b). This may be due to the effect of pressure and or temperature on Zr partitioning between Opx and liquid, as discussed in the text. The value used is intermediate between the two estimates in Table 2).
- \*\* A lower value of  $D(\text{Zr})$  garnet/liquid than determined in this study is adopted based upon other ion probe studies of Zr in garnet lherzolites in our laboratory.

piled from studies on the Woods Hole ion microprobe [23,26,35, and our unpublished studies of the experiments of McKay, 36]. Thus, while the partition coefficients for the REE from Nd to Yb, and for Zr and Ti, are quite similar to those compiled by Kelemen et al. [21], in this data set rare earths were measured in the same samples as other trace elements, all by the same technique. Note that garnet/Cpx and garnet/basaltic liquid distribution coefficients for Zr are very similar to those for Ti [35,37,38], resulting in higher  $D_{Zr}^{garnet/liq}$  than for Nd and Sm, and lower  $D_{Ti}^{garnet/liq}$  than for Gd and Dy, as has also been shown for garnet/high silica rhyolite [39].

The new data for La and Ce are in accord with many previous studies [e.g., 23–25,35–40 and references cited in 21,22]. New data for K are in qualitative agreement with previous data [e.g., 41], indicating very large partition coefficients for K in Cpx/garnet and Cpx/Opx pairs. However, we are concerned by discrepancies in our data for Zr in Opx. It is fairly well established that  $D_{Zr}^{Opx/Cpx}$  is about 0.2 in spinel and plagioclase lherzolites and harzburgites [21,23,24]. In contrast,  $D_{Zr}^{Opx/Cpx}$  in garnet lherzolites in this study is

consistently less than 0.1, averaging roughly 0.04 (Table 2b). In subsequent modeling, we have used a value of 0.014, intermediate between the “low pressure”  $D_{Zr}^{Opx/liq}$  from previous studies and our analyses of experimental samples (0.02, Table 2a), and the “high pressure”  $D_{Zr}^{Opx/liq}$  from garnet lherzolites (0.006, Table 2b). The result is that Zr is *not* strongly fractionated from Nd and Sm by Opx in our calculations.

For modeling purposes, it was necessary to estimate distribution coefficients for K, Nb and REE in spinel. We assumed that spinels essentially exclude K, and used Stosch’s values [42] for mantle spinel/clinopyroxene, multiplied by Hart and Dunn’s clinopyroxene/basaltic liquid distribution coefficients, for the REE. Mantle spinels almost certainly contain significant quantities of Nb relative to co-existing anhydrous silicate minerals. To estimate  $D_{Nb}^{spinel/liq}$ , we used a ratio of  $D(Ti)/D(Nb)$  of about 15, determined for spinels ranging from magnetite to spinel–chromite solid solutions grown in Nb-doped basaltic liquids [Nielsen, pers. commun., 1993]. This ratio, combined with Kelemen et al.’s [21] estimate for  $D(Ti)$  in mantle spinel/basaltic liquid of 0.15,

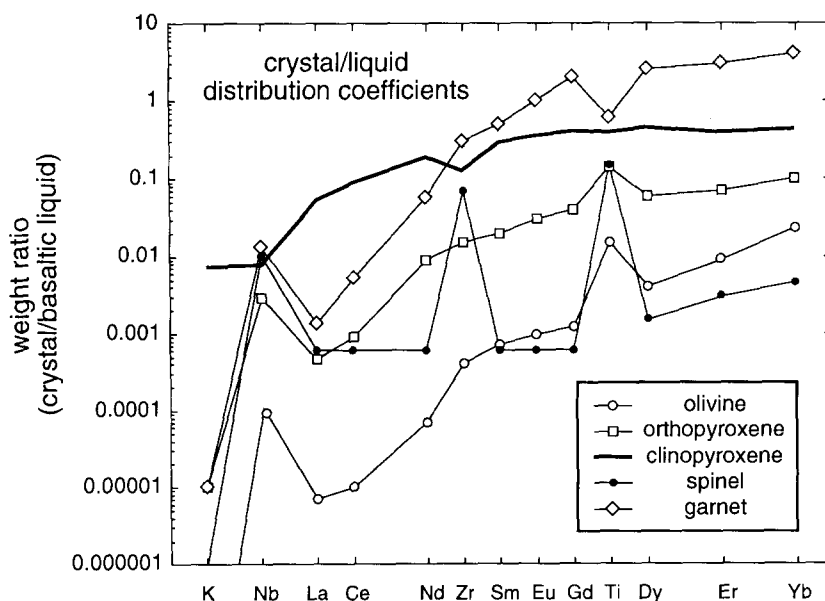


Fig. 4. Illustration of partition coefficients used in modeling (Table 3). Note fractionation of Nb, Zr and Ti from the REE and K in Opx, garnet, spinel and olivine. See text, Figs. 2 and 3, and Tables 2 and 3 for additional information.

Table 4  
Phase proportions, bulk distribution coefficients and chondrite-normalized bulk compositions used in modeling

Bulk Distribution Coefficients												
	peridotite melt mode spinel lherzolite facies	peridotite melt mode gamet lherzolite facies	basalt melt mode and bulk D's eclogite facies without rutile	basalt melt mode and bulk D's eclogite facies with rutile	spinel pyrolite bulk distribution coefficients	gamet pyrolite bulk distribution coefficients	spinel harzburgite product bulk D's Fig. 6A	gamet harzburgite product, bulk D's Fig. 6A,7C	spinel harzburgite product bulk D's Fig. 6B&C	Opx-rich spinel harzburgite product Figs. 7A,B&D	dunite product bulk D's Fig. 7C	ortho- pyroxenite product bulk D's Fig. 7C
notes	1	1	1,2	1,2,3	4	4						
K	.0065	.0021	.0032	.0032	.0013	.0007	.000002	.000003	.000002	.000005	.000000001	.00001
Nb	.0098	.0085	.0087	.1586	.0034	.0043	.0012	.0013	.0010	.0019	.0006	.0033
La	.0485	.0165	.0247	.0247	.0096	.0053	.0001	.0002	.0001	.0002	.000037	.0005
Ce	.0776	.0277	.0406	.0406	.0154	.0092	.0002	.0004	.0002	.0004	.000040	.0009
Nd	.1714	.0811	.1060	.1060	.0356	.0303	.0019	.0047	.0014	.0041	.0001	.0086
Zr	.1294	.1661	.1633	.3635	.0311	.0734	.0066	.0181	.0059	.0100	.0039	.0168
Sm	.2677	.3015	.3100	.3099	.0573	.1297	.0046	.0295	.0036	.0094	.0007	.0190
Eu	.3237	.5327	.5135	.5134	.0706	.2358	.0067	.0567	.0053	.0140	.0009	.0285
Gd	.3716	.9732	.8880	.8878	.0823	.4400	.0089	.1089	.0070	.0186	.0012	.0380
Ti	.4112	.3939	.4105	-	.1244	.1855	.0465	.0690	.0403	.0773	.0218	.1391
Dy	.4145	1.2014	1.0859	1.0856	.0966	.5476	.0151	1.400	.0123	.0291	.0039	.0571
Er	.3663	1.3994	1.2382	1.2378	.0921	.6457	.0209	1.708	.0179	.0362	.0087	.0667
Yb	.4087	1.8428	1.6135	1.6130	.1146	.8599	.0375	2.373	.0336	.0567	.0221	.0952
modal proportions, wt%												
olivine	40	10	0	0	46	54	75	75	80	50	95	0
Opx	30	18	20	19.5	28	17	20	20	15	4.5	0	95
Cpx	90	30	45	4.5	18	9	0	0	0	0	0	0
spinel	20	0	0	0	8	0	5	0	5	5	5	5
gamet	0	42	35	35	0	20	0	5	0	0	0	0
rutile	0	0	0	0.5	0	0	0	0	0	0	0	0
Chondrite Normalized Bulk Compositions												
	pyrolite Hofmann NMORB	Sun & McDonough NMORB	15% melt gamet pyrolite liquid reactant Fig. 6A	05% melt gamet pyrolite liquid reactant Fig. 6B&C	2.0% melt of basalt w rutile liquid reactant Fig. 7A,C,D	residue 19% batch melting spinel pyrolite solid reactant Fig. 6,7D	19% batch melting spinel pyrolite solid reactant Fig. 6,7D	C1 chondrite normalization factors (ppm)				
	5	6	6	7	7	3,7	7	8				
1	14.3	9.7	63.8	175.2	711.3	.0002		62.0				
1.1	14.3	9.5	62.6	144.1	85.2	.0061		246				
1.3	16.6	10.7	64.2	124.0	463.8	.0029		2347				
1.5	19.9	12.4	63.2	106.3	389.9	.0055		6032				
1.6	24.7	16.1	40.1	51.9	214.4	.0255		4524				
1.7	26.5	18.8	29.1	34.1	71.5	.0587		3.94				
1.8	25.5	17.9	19.0	20.6	80.5	.0587		1471				
1.9	23.8	16.2	12.7	13.2	46.0	.0866		.056				
2	25.8	18.7	7.9	8.0	29.1	.1158		1966				
2	22.2	17.4	13.8	14.5	26.5	.3914		436.0				
2	26.0	18.7	6.5	6.5	23.9	.1718		2427				
2	26.1	18.7	5.6	5.6	21.1	2.118		1589				
2	24.0	18.8	4.2	4.2	14.9	.3256		1625				
46	0	0	10	10	0	68						
28	20	20	18	18	19.5	27						
18	45	45	30	30	45	0.5						
8	0	0	0	0	0	4.5						
0	35	35	42	42	35	0						
0	± 0.5	± 0.5	0	0	0.5	0						

yields an approximate  $D_{\text{Nb}}^{\text{spinel/liq}}$  of 0.01, the same as that determined directly by Nielsen for Cr-rich spinels.

We caution the reader that the present set of partition coefficients remains approximate. As stated above, the estimates for  $D^{\text{crystal/liq}}$  for K and La in Opx and garnet, and for Ce in Opx, are maximum values. Perhaps more importantly, we cannot account for the effects of pressure, temperature and bulk composition on trace element exchange equilibria. However, our main focus in this paper is fractionation of one incompatible element from another, rather than the absolute concentration of specific elements in specific liquids. Whereas individual partition coefficients for REE and Ti between Cpx and liquid are quite variable, depending upon liquid composition, the ratios of these partition coefficients are nearly constant in crystal/liquid equilibria involving basaltic to andesitic magmas [e.g., 43]. Thus, we believe that fractionation of inter-element ratios is likely to be a robust result of the modeling presented in subsequent sections of this paper.

## 6. Modeling of melting

The distribution coefficients from Table 3 were used in melting models based on Gast [44] and

Shaw [45]. Table 4 provides details of the parameters used, and Fig. 5 illustrates some of the results. Fractional melting of fertile lherzolite [pyrolite, 46] in spinel lherzolite and garnet lherzolite facies does not significantly fractionate Nb from K and La (Fig. 5a). In addition, the fractionation of Ti from Gd and Dy in garnet creates a Ti enrichment relative to the REE in liquids produced by melting of garnet lherzolite. This effect is quite marked, and may be evident in melts derived exclusively from garnet lherzolites. Melting of harzburgites is not illustrated here. There will be a change in the proportion of phases entering partial melts when Cpx is exhausted from the source; fractionation of Nb from La and K during melting will occur in the absence of Cpx. However, melting of depleted harzburgite is not a viable process for generating subduction-related magmas, since the concentrations of all incompatible elements would be too low to produce liquids with light REE and K higher than in mid-ocean ridge basalts.

Melting of basalt to produce an eclogite residue without rutile does not produce fractionation of Nb from La and K, even in very small melts. Following the suggestion of Ryerson and Watson [1], we modeled melting of basalt with residual rutile-bearing eclogite, and the results are pre-

---

### Notes to Table 4

Bulk distribution coefficients calculated using the phase proportions reported here and the mineral/basaltic liquid coefficients in Table 3. See text for further discussion of modeling.

<sup>1</sup> Peridotite and eclogite melt modes calculated using the high-pressure norm method of Kelemen et al. [22]. Negative olivine in the spinel lherzolite facies indicates incongruent melting to form olivine + liquid.

<sup>2</sup> Melting of basaltic bulk compositions in eclogite facies is assumed to be nearly eutectic, as approximately observed in the results of Rapp et al. [18].

<sup>3</sup> Fixed distribution coefficients should not be used for Ti in melting and melt/rock equilibria where liquid is saturated in rutile [1]. Ti content in liquids produced by eclogite with 0.5% rutile in source composition and melt mode were estimated to yield a smooth trend from Gd to Dy. Estimates are within the limits of the data of Rapp et al. [18].

<sup>4</sup> Pyrolite modes calculated from the major element composition of pyrolite [46] using the high-pressure norm method of Kelemen et al. [22].

<sup>5</sup> Approximate trace element composition of MORB pyrolite based on chondritic abundances (core) and isotopic and trace element composition of NMORB [see 6,9,46,71].

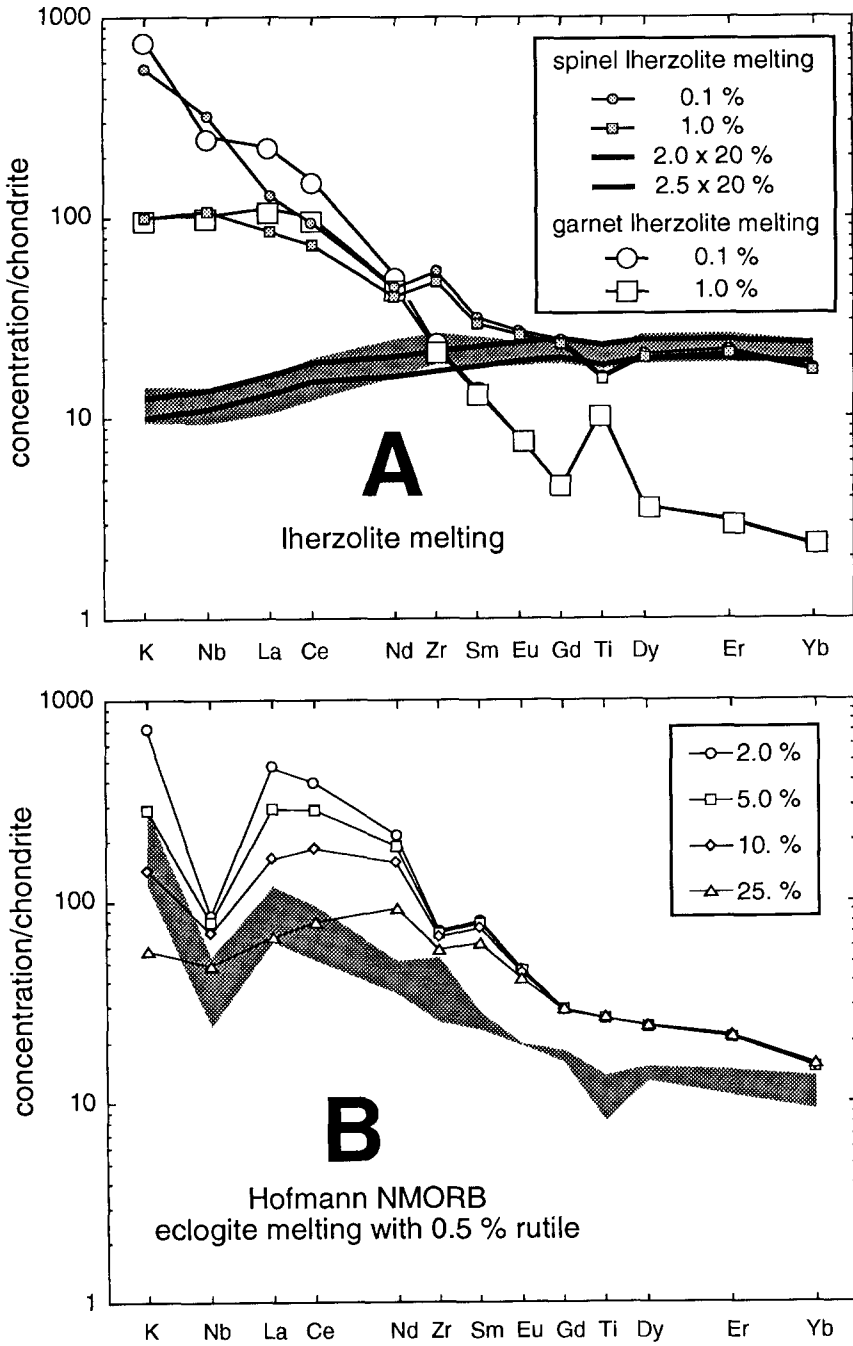
<sup>6</sup> Normal mid-ocean ridge basalt (NMORB) trace element compositions from Hofmann [6] and Sun and McDonough [7]. Mode is approximate, based on high-pressure norm method of Kelemen et al. [22].

<sup>7</sup> Results of batch melting calculations. Although fractional melting models fit the composition of residual peridotite from oceanic fracture zones to a first approximation, in detail, fractional melting models are inappropriate analogues to natural melting processes at very low degrees of melting [55,56].

<sup>8</sup> C1 chondrite normalization factors from Anders and Grevesse [69]. Normalization factor for K is nine times C1 chondritic abundance.

sented in Fig. 5b. When basalt melts with 0.5 wt% rutile in the initial mode and the melt mode [18], and  $D_{Nb}^{rutile}$  of 30 [20], Nb is very strongly

fractionated from K and La, producing substantial Nb depletion. Because the  $TiO_2$  content is buffered in partial melts with rutile in their



residua [1], we cannot use trace element distribution coefficients to calculate its abundance in these melts. Rapp et al. [18] found 10–30 times chondritic abundances of Ti in rutile saturated partial melts of hydrous metabasalts at 22–32 kbar, with the concentration of Ti increasing with increasing temperature. We have used values in this range, along a smooth variation trend between Gd and Dy, in subsequent modeling incorporating small-degree melts of basalt.

Despite the potential fractionation of Nb from La and K caused by residual rutile, slab melts are not appropriate parental liquids for most arc magmas, or for the continental crust. As noted by Gill [47] and many subsequent workers, small-degree partial melts of basalt with residual eclogite have La/Yb ratios higher than in the continental crust, too high to be parental to most arc magmas. In addition, our review in a subsequent paper will show that high-Mg# andesites and the continental crust have a Mg#, Ni content, and Cr content higher than andesitic liquids produced by partial melting or crystal fractionation from basaltic compositions.

We emphasize that the model for basalt melting is semi-quantitative. The rutile mode is not well constrained, and could be less than 0.5 wt%. Ongoing experiments by one of us (Dunn) will provide more quantitative data on rutile abundance during melting of hydrous basalts. Secondly, incompatible elements generally become more compatible in Cpx with increasing SiO<sub>2</sub>

content in calc-alkaline magmas [28,43,48]. Values for  $D^{Cpx/liq}$  larger than those in Table 3 could be used to model partial melting of hydrous metabasalt to form magmas with 60–70 wt% SiO<sub>2</sub>. However, the results are surprisingly insensitive to doubling  $D^{Cpx/liq}$ , which does not change La/Yb, and decreases REE abundances in calculated liquids by less than 10% in all the cases illustrated. Comparison of  $D^{garnet/liq}$  for basaltic magmas to data for garnet in silicic melts [39 and references cited therein] suggests that the middle to heavy REE become far more compatible with increasing SiO<sub>2</sub>. If we incorporated this effect in modeling, the La/Yb slope of partial melts would be even higher than in Fig. 5b, increasing the mismatch between high pressure, partial melts of basalt and the composition of the continental crust. Instead, for simplicity, we have used the same  $D^{Cpx/liq}$  and  $D^{garnet/liq}$  values throughout this paper.

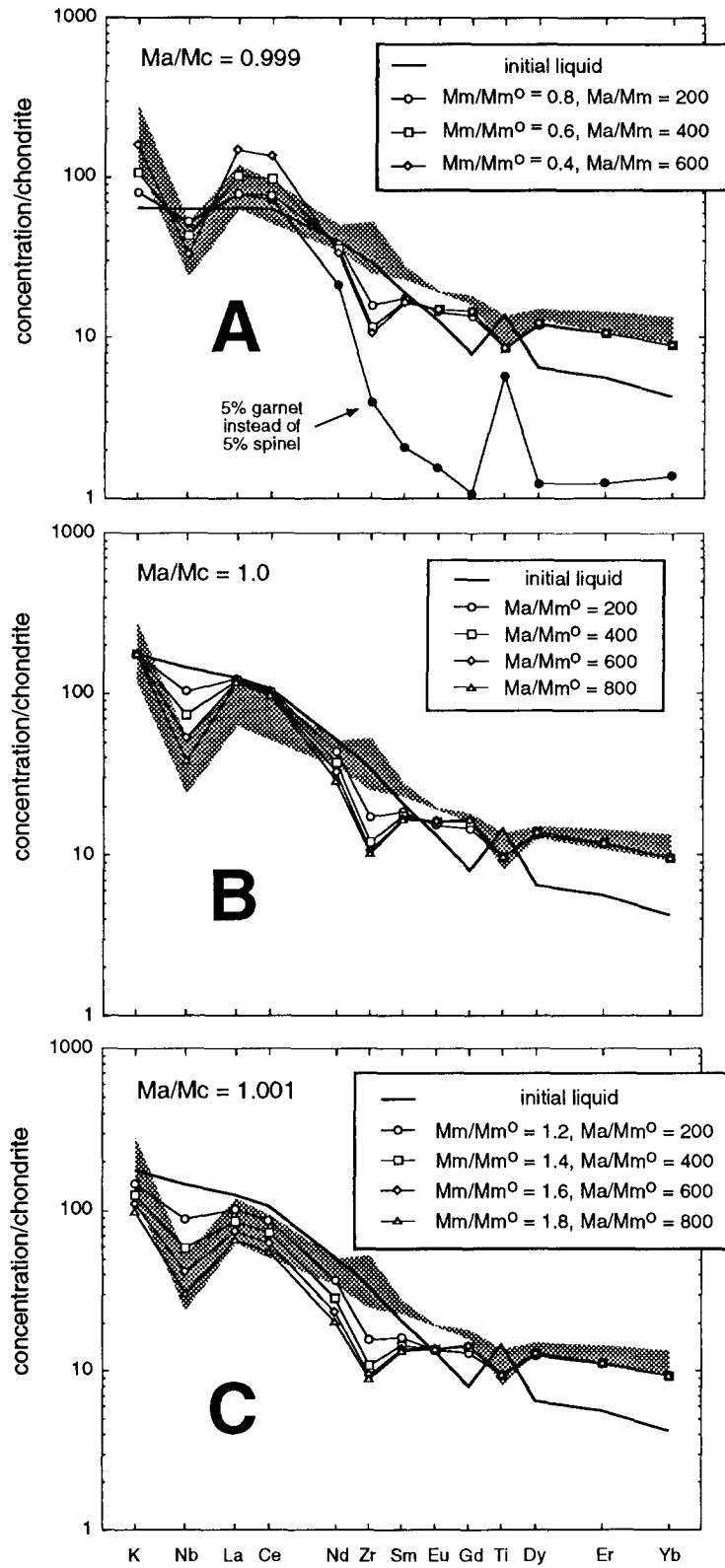
## 7. Modeling of melt/rock reaction in the upper mantle

### 7.1. General considerations

The mineral/melt partition coefficients from Table 3, combined with phase equilibrium considerations, allow us to make semi-quantitative models of melt/rock reaction in the upper mantle and to study the effect of such an open system in

---

Fig. 5. A. Melting models for mantle peridotite in spinel and garnet lherzolite facies. Calculated liquid compositions are reported, normalized to concentration in C1 chondrite (except K; see caption for Fig. 1). Hachured field is range of estimated average compositions for normal MORB [6,9], from Fig. 1. Initial composition is "pyrolite" [46], with trace element characteristics suitable for the MORB source (Table 4). Melting modes are based on the norm calculations of Kelemen et al. [22] for experimental liquids reported to be in equilibrium with lherzolite. In the modeling results note the absence of significant fractionation of Nb from La and K, even at very low degrees of melting, and the presence of a pronounced Ti enrichment in melts of garnet lherzolite. For this and subsequent illustrations of modeling results, distribution coefficients are listed in Table 3, and quantitative source and reactant compositions are compiled in Table 4. For melting of spinel lherzolite, additional curves are shown for 2 and 2.5 times the calculated liquid composition for 20% melting of pyrolite. These correspond closely to the composition of normal MORB and could be formed by crystal fractionation from a 20% melt of pyrolite, or by melting of a source with the major element composition of pyrolite but roughly twice the abundance of incompatible trace elements used here. B. Melting models for basalt at high pressure, with 0.5% rutile in the source and melt modes. Initial composition from Hofmann [6]. Melting modes are eutectic, in accord with the experimental results of Rapp et al. [18]. Hachured field is the range of estimated average compositions for the continental crust [4,5], from Fig. 1. Strong fractionation of Nb from La and K is produced in the melting models with rutile, but middle to light REE abundances are much too high to reproduce the observed composition of the continental crust. Distribution coefficients in Table 3, source compositions in Table 4.



fractionating Nb from La and K in derivative liquids. The reaction model used in this study is the AFC formulation of DePaolo [49], similar to the original zone refining model of Harris [50]. It is different from “chromatographic” models [51–53] in that the AFC monitors the composition of a single batch of liquid as a function of reaction progress, while chromatographic models monitor the composition of a fixed volume of peridotite as it reacts with successive infiltrating liquids. These methods produce similar results for liquid compositions, provided diffusion is not an important factor, and if the phase proportions are constant during reaction. If diffusion is to be included, or where mantle composition is to be monitored during continuous reaction with migrating melt, the chromatographic approach is preferable. On the other hand, AFC models lend themselves to changes in solid and liquid phase proportions, as well as the trace element compositions of the phases.

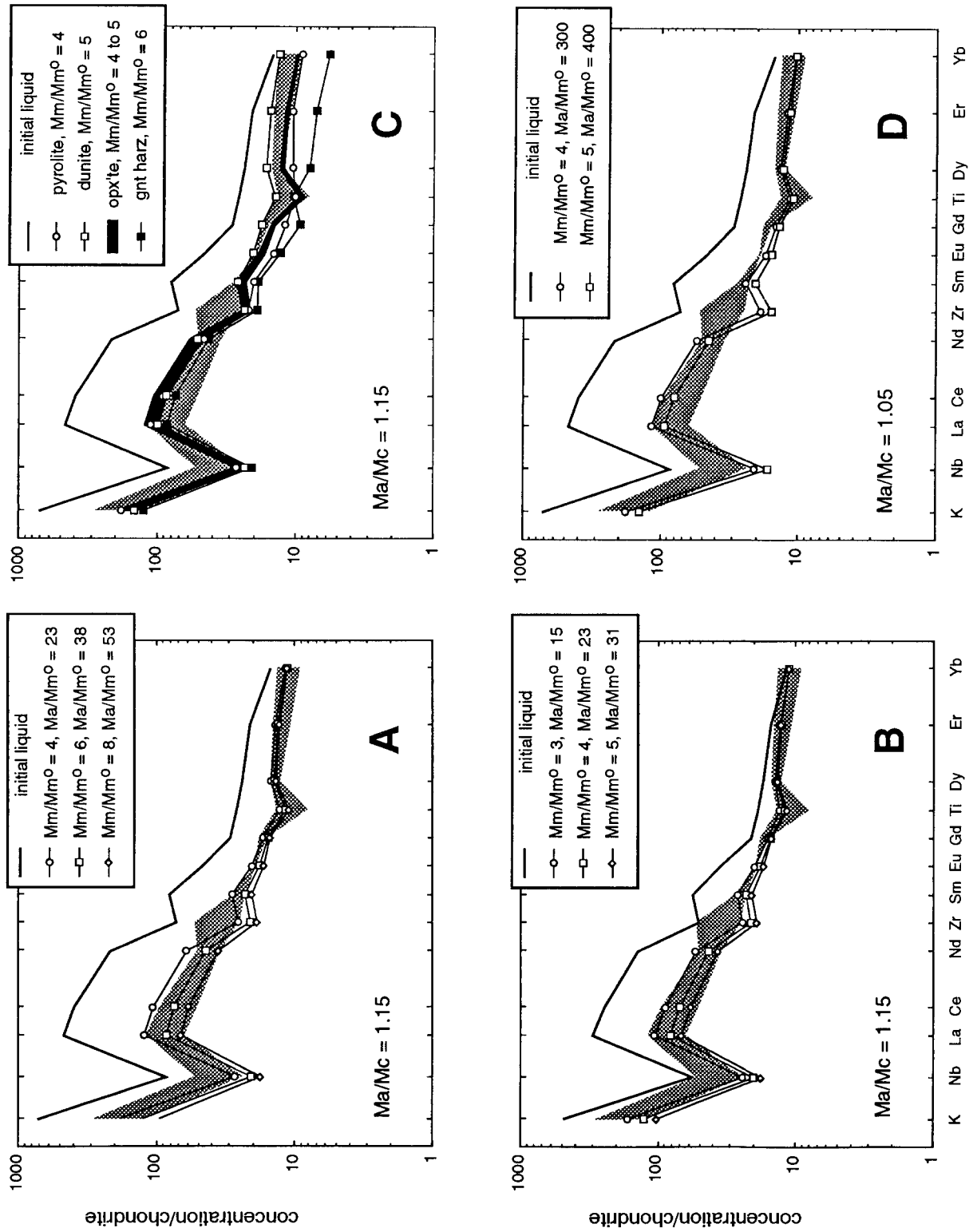
### 7.2. Reaction between mantle-derived magmas and depleted harzburgite

In this section, we present results of modeling the reaction between ascending, mantle melts and depleted harzburgite (Table 4, Fig. 6). Nb depletion relative to La and K can be produced by interaction between liquid, olivine, Opx and spinel. We initially used a model in which Cpx was dissolved and olivine and Opx produced, by reaction between lherzolite and liquid to create harzburgite, as in [22]. This modeling was appar-

ently successful, in that it produced a close match to the trace element composition of the continental crust (better than in Fig. 6), but the melt/rock ratios were very small. We doubt that Cpx dissolution reactions can continue indefinitely in ascending melts in the mantle, without eventually producing a Cpx saturated liquid product.

Thus, we modified our approach, and investigated the reaction between ascending liquid and residual harzburgite, in which the proportions of olivine, pyroxene and spinel in the harzburgite are hardly modified at all (Table 4). Ascending melts interacting with harzburgite can react indefinitely without saturation in Cpx [22,54]. The liquid mass will increase under conditions of near-adiabatic decompression, and decrease if the liquid is cooling. HFSE are fractionated from LILE and REE as the liquid gradually loses trace elements: by dissolution of depleted harzburgite where liquid mass is increasing, crystallization of enriched harzburgite where liquid mass is decreasing, and in exchange reactions with incompatible, element-depleted olivine, Opx and spinel. Very small melt/rock ratios are necessary to produce substantial Nb depletion by mantle/magma interaction, and this causes the middle and heavy REE to approach steady-state values in equilibrium with the harzburgite reactant. Since the harzburgite reactant is previously depleted by melting, the middle REE in derivative liquids are too low for the bulk continental crust, although they are appropriate for some high-Mg# andesites (Fig. 1). If the harzburgite reactant was formed by a melt/rock reaction [22]

Fig. 6. Results of modeling reaction between small degree melts of garnet lherzolite with depleted spinel harzburgite in the upper mantle. Calculated liquid compositions are reported, normalized to concentration in C1 chondrite (except K; see Fig. 1). In the top diagram, the initial liquid is a 1.5% melt of garnet pyrolyte; in the bottom two diagrams, the initial liquid is a 0.5% melt of the same source composition. Hachured field is the range of estimates of continental crust composition, from Fig. 1. In this and subsequent illustrations of results of melt/rock reaction modeling, three input parameters are specified on the diagrams:  $Mm/Mm^0$  refers to the liquid mass produced relative to the mass of the initial liquid.  $Ma/Mm^0$  refers to the mass of peridotite “assimilated” relative to the mass of the initial liquid. This is equivalent to the integrated ratio of solid/liquid reactants and is the reciprocal of the integrated melt/rock ratio.  $Ma/Mc$  refers to the mass “assimilated” relative to the mass crystallized. If this value is greater than 1, the mass of solid reactants is less than the mass of solid products, and liquid mass will increase as a function of reaction progress. If it is less than 1, the liquid mass will decrease. Distribution coefficients in Table 3, reactant and product compositions in Table 4. A. The effect of having garnet, rather than spinel, in the harzburgite reactant and product assemblage is illustrated by the single, labeled curve. Interaction between garnet and liquid lowers heavy REE concentrations and creates Ti enrichments relative to Eu and Dy in derivative liquids.



instead of by melting, the middle REE in derivative liquids would not be so depleted, and perhaps a closer match to continental crustal compositions could be achieved. This is an area of continuing investigation.

### 7.3. Mass balance for magma / mantle interaction

The melt/rock ratios requisite to form Nb depletions are very small, less than or equal to 0.005. While these values are model-dependent to some degree, a large mass of solid relative to liquid reactants is a necessary part of the Nb fractionation process. Thus, the question arises whether the mantle underlying subduction-related magmatic arcs has sufficient mass to produce Nb fractionation. Melt transport by porous flow requires very small melt/rock ratios. Chemical and physical estimates of the porosity in peridotite which is likely to be maintained during porous flow range from about 0.1 to 5 wt% [55–57]. Even if the higher estimate is correct, 1 m<sup>3</sup> of liquid will be distributed through 20 m<sup>3</sup> of peridotite and need only pass through ten such volumes to achieve a melt/rock ratio of 0.005. Therefore, on the scale of a single melt fraction migrating by porous flow, melt/rock ratios on the order of 0.005 are easily attainable.

Can melt/rock ratios of 0.005 be sustained during formation of the entire crust in a subduction-related magmatic arc? For simplicity, the following calculation assumes that each volume of mantle peridotite can react with only one batch of ascending liquid to fractionate Nb from La and K. All liquid migrates upward to form arc crust. Melt ascends through the mantle by pervasive grain boundary infiltration through the entire

wedge. With these assumptions, the question of melt/rock ratio becomes a simple mass balance between the igneous arc crust and the underlying mantle wedge. Estimates of the production rate of volcanic rocks over short time intervals [58] range from 3 to 10 m<sup>2</sup>/yr per unit length of arc. If these represent half the mass of liquids passing through the Moho, then the total magmatic flux might be 6–20 m<sup>2</sup>/yr. If corner flow, bringing new material into the mantle wedge above the subducting slab, occurs at an average velocity of 4 cm/yr [e.g. 59] over a depth interval of 50 km, this could deliver 2000 m<sup>2</sup>/yr of peridotite to react with ascending melts. Ignoring the difference in density between mantle peridotite and arc crust, this gives a total melt/rock mass ratio of 0.003–0.01.

Another way to estimate the net flux is to measure the cross-sectional area of arc crust, subtract the contributions of pre-existing crustal basement and accretionary prisms, and then divide by the duration of arc magmatism. Using the Aleutian cross-section of Grow [60], we estimate that the igneous material added to the Bering Sea crust in the Aleutians averages a thickness of 8 km over a width (parallel to the subduction direction) of 100 km. This material was produced over about 80 million yr, yielding a flux of 10 m<sup>2</sup>/yr, in accord with an estimated total crustal magmatic budget of 12 m<sup>2</sup>/yr for the Peruvian arc by Brown [61]. Combining this estimate with the mantle flux due to corner flow in the wedge (previous paragraph) leads to an estimated melt/rock ratio of 0.005. Thus there may be (barely) sufficient mantle material delivered to the wedge to create Nb depletions in all arc magmas as a result of a single-pass reaction process.

Fig. 7. Results of modeling reaction between small degree melts of high pressure basalt and mantle peridotite, producing spinel harzburgite with increasing liquid mass. Liquid compositions are reported, normalized to concentration in CI chondrite (except K; see Fig. 1). See caption to Fig. 6 for description of the variables reported on these diagrams. Hatched field is the range of estimates of continental crust composition, from Fig. 1. A. A 2% melt of normal MORB, with 0.5% rutile in the source, reacts with lherzolite (pyrolite). B. The Sun and McDonough [9] estimate for normal MORB composition is substituted for that of Hofmann [6]. C. The reactants are the same as in A, but the solid product composition is varied; results are presented for solid products including lherzolite (pyrolite), dunite, orthopyroxenite and garnet harzburgite. D. The rate of increase in magma mass is smaller, and a 2% melt of the Hofmann MORB composition reacts with the same depleted harzburgite used as a reactant in modeling presented in Fig. 6. Distribution coefficients in Table 3, reactant and product compositions in Table 4.

#### 7.4. Reaction between slab-derived melt and the upper mantle

The crystal/liquid distribution coefficients in Table 3 have also been used to model reaction between mantle peridotite and slab-derived, partial melts with a rutile-bearing, eclogite residue. Interaction between slab melts and peridotite in the mantle wedge has been suggested as a potentially important process in arc petrogenesis [e.g. 1,62,63]. Such interaction might metasomatize the mantle, producing hybrid peridotite which could later melt to form arc magmas [1,62], alternatively, interaction might produce hybrid liquids which are directly parental to some arc magmas [63]. Whatever the origins of arc magmas (by slab and/or mantle melting), they must pass through an inverted geotherm until they reach the temperature of the thermal maximum in the wedge, some 1100–1300°C at about 75 km [59,64]. This creates an otherwise unusual situation in which ascending melts must heat up during decompression. Increasing liquid temperature, combined with decreasing pressure, in an open system, provides substantial thermal energy for crystal dissolution.

Rising slab melts which are heated as they interact with the mantle will dissolve peridotite, increasing in mass, until they become saturated in hornblende, pyroxene and/or olivine. If initial saturation is with hornblende or Opx, the fate of the liquid depends largely upon the rate of reaction versus the rate of continuing decompression and heating. If decompression and heating are slow relative to reaction rates, some liquids may be consumed by reactions in which liquid + olivine form Opx and/or hornblende. However, if initial saturation is with olivine, or if decompression and heating are fast relative to reaction rates (due to rapid magmatic ascent or to partial armouring of magmatic conduits with hornblende and pyroxene), then liquid mass will continue to increase. Thus, depending upon the water and alkali contents of these liquids, the rate of reaction versus decompression, and the nature of the wedge geotherm, hybrid magmas may continue to react with peridotite, heating until they reach the ther-

mal maximum in the wedge, and then cooling as they continue to ascend.

Our modeling, presented in Fig. 7, demonstrates the effects of reaction with increasing liquid mass on the trace element contents of hybrid liquids. It is remarkably easy to reproduce the trace element composition of the continental crust via modeling of this process. While melt mass increases by a factor of 3–8, magma–mantle reaction reduces the La/Yb ratio of the high-pressure basalt partial melts to values observed in high-Mg# andesites and in the continental crust, produces depletion of Ti relative to Eu and Dy, and retains the Nb depletion inherited from slab melting in the presence of rutile. Required melt/rock ratios range from 0.05 to 0.02 in most cases. The general features of this model are very robust. In Fig. 7, we illustrate the effects of varying initial liquid composition (A and B), product solid composition (A and C), and reactant composition (A and D). All combinations produce a similarly good fit to the composition of high-Mg# andesites and the continental crust. It should be added that the reaction of slab melts with mantle peridotite, under conditions of increasing liquid mass, will elevate the Mg#, and Ni and Cr contents, of derivative liquids to values appropriate for equilibrium with mantle olivine and spinel.

A simple mass balance for this process illustrates that it will not be limited by the availability of reactants. The initial liquid used in modeling is a 2% melt of basalt. For a 6 km thick slab subducting at 5 cm/yr, this corresponds to a melt production rate of 6 m<sup>2</sup>/yr, if the entire crust undergoes anatexis. Increasing this by a factor of 3–8, due to the dissolution of mantle minerals, forms 18–48 m<sup>2</sup>/yr of hybrid magma, an ample quantity to supply the magmatic flux to an active volcanic arc. As illustrated in the preceding discussion of mass balance for mantle/magma interaction, supply of peridotite in a steady state, convecting wedge can easily sustain melt/rock ratios greater than 0.01.

Many substantial objections may be raised in considering this scenario:

(1) Can a small-degree melt segregate from the slab and rise into the overlying mantle wedge?

Melts of hydrous metabasalt, rich in H<sub>2</sub>O and alkalis, have a low viscosity and a small pyroxene/liquid wetting angle [65 and B. Watson, pers. commun., 1993], and might, therefore, be capable of segregating from their residua by porous flow along an interconnected grain boundary network.

(2) Does the slab actually melt? The most recent models for subduction zone *PT* paths suggest that slab melting is common only when very young (hot) ocean crust is subducting, and/or during initiation of a new subduction zone while the mantle wedge remains hot [63,64]. Such conditions may have been more common in the Archean, when the Earth's deep interior was warmer, producing steeper, near-surface geotherms and/or faster rates of plate tectonics [e.g., 66]. Another possibility is that metasediments form small-degree melts which rise into the mantle wedge [67]. By analogy to eutectic melting behavior in simple systems, perhaps mixtures of metabasalt and sediments have even lower melting temperatures than the individual end members. Provided such melts are saturated in rutile, and not in minor phases which retain REE in their residua, they could be appropriate reactants in the general scheme outlined in this section.

## 8. Conclusion

Previous work has shown that melt/rock reaction in the upper mantle can produce liquids with the major element characteristics of high-Mg# andesites [54,68], similar to the bulk composition of the continental crust [4,5]. In addition, melt/rock reaction can account for high concentrations of Opx, high light/heavy rare earth element ratios, and fractionation of Ti from the rare earth elements in the sub-continental lithosphere [22]. In this paper, we have illustrated two general models in which melt/rock reaction in the upper mantle can produce the trace element characteristics of high-Mg# andesite magmas and the continental crust. In a forthcoming paper, we explore alternative models for generation of the continental crust. The results of experimental petrology

illustrate that high-Mg# andesites, with compositions similar to that of the continental crust, are probably not produced by partial melting of mantle peridotite, nor by melting or crystal fractionation from basaltic bulk compositions. Instead, it is likely that melt/rock reaction has been an important process in forming high-Mg# andesites.

We infer that the compositional similarity between high-Mg# andesites and the continental crust is not a coincidence. Although basaltic magmas predominate among volcanic rocks in contemporary intra-oceanic arcs, high-Mg# andesites may have been more common in the past, they may be selectively produced in specific arc environments (such as ridge subduction), they may be selectively preserved during later erosion and plate collision and they may be more common among plutonic rocks than they are among volcanic rocks in arcs. As a result of some combination of these factors, continental crust may have been produced by accretion of mantle-derived, high-Mg# andesite magmas.

## Acknowledgments

We wish to thank Ken Burrhus for his indefatigable assistance with the Woods Hole ion microprobe, Joe Boyd and Tony Erlank for providing Kapvaal garnet lherzolite samples, Stan Hart for many illuminating discussions on andesites and crustal genesis, Roger Nielsen for sharing unpublished data on partitioning between spinel and liquid, Sue and Bob Kay for their compilation of Aleutian data [8, in press], Claude Dupuy for a critical reading, and Terry Plank, N.W. Rogers and S.M. Eggins for thorough, constructive reviews which resulted in substantial improvement of this paper.

## References

- [1] F.J. Ryerson and E.B. Watson, Rutile saturation in magmas: Implications for Ti–Nb–Ta depletion in island-arc basalts, *Earth Planet. Sci. Lett.* 86, 225–239, 1987.
- [2] J.A. Pearce and J.R. Cann, Tectonic setting of basic volcanic rocks determined using trace element analyses, *Earth Planet. Sci. Lett.* 19, 290–300, 1973.

- [3] J.-L. Joron and M. Treuil, Utilisation des propriétés des éléments fortement hygromagmatophiles pour l'étude de la composition chimique et de l'hétérogénéité du manteau, *Bull. Soc. Geol. Fr.* 19, 1197–1205, 1977.
- [4] S.R. Taylor and S.M. McLennan, *The Continental Crust: Its Composition and Evolution, An Examination of the Geochemical Record Preserved in Sedimentary Rocks*, 312 pp., Blackwell, Oxford, 1985.
- [5] B.L. Weaver and J. Tarney, Major and trace element composition of the continental lithosphere, *Phys. Chem. Earth* 15, 39–68, 1984.
- [6] A.W. Hofmann, Chemical differentiation of the Earth: the relationship between mantle, continental crust, and oceanic crust, *Earth Planet. Sci. Lett.* 90, 297–314, 1988.
- [7] R.L. Rudnick and T. Presper, Geochemistry of intermediate to high-pressure granulites, in: *Granulites and Crustal Evolution*, D. Vielzeuf and P. Vidal, eds., pp. 523–550, Kluwer, Dordrecht, The Netherlands, 1990.
- [8] S.M. Kay and R.W. Kay, Aleutian magmas in space and time, in: *The Geology of Alaska*, G. Plafker and H.C. Berg, eds., in press, Geol. Soc. Am., Boulder, Colo., 1993.
- [9] S.-S. Sun and W.F. McDonough, Chemical and isotopic systematics of oceanic basalts: Implications for mantle composition and processes, in: *Magmatism in the Ocean Basins*, Geol. Soc. Spec. Publ. 42, 313–345, 1989.
- [10] A.D. Saunders, J. Tarney, N.G. Marsh and D.A. Wood, Ophiolites as ocean crust or marginal basin crust: A geochemical approach, in: *Ophiolites: Proceedings of the International Ophiolite Symposium*, A. Panayiotou, ed., pp. 193–204, Nicosia, Cyprus, 1980.
- [11] C.J. Hawkesworth, K. Gallagher, J.M. Hergt and F. McDermott, Trace element fractionation processes in the generation of island arc basalts, *Philos. Trans. R. Soc. London A* 342, 179–191, 1993.
- [12] Y. Tatsumi, D.L. Hamilton and R.W. Nesbitt, Chemical characteristics of fluid phase released from a subducted lithosphere and origin of arc magmas: evidence from high-pressure experiments and natural rocks, *J. Volcanol. Geotherm. Res.* 29, 293–309, 1986.
- [13] J.C. Ayers and E.B. Watson, Solubility of apatite, monazite, zircon, and rutile in supercritical aqueous fluids with implications for subduction zone geochemistry, *Philos. Trans. R. Soc. London A* 335, 365–375, 1991.
- [14] J.M. Brennan and E.B. Watson, Partitioning of trace elements between olivine and aqueous fluids at high P–T conditions: Implications for the effect of fluid composition on trace-element transport, *Earth Planet. Sci. Lett.* 107, 672–688, 1991.
- [15] H.A. Randle and N.W.A. Odling, Experimental evidence for the role of fluids in subduction zones, *EOS Trans. Am. Geophys. Union* 73, 637–638, 1992.
- [16] L. Briquieu, H. Bougault and J.-L. Joron, Quantification of Nb, Ta, Ti and V anomalies in magmas associated with subduction zones: Petrogenetic implications, *Earth Planet. Sci. Lett.* 68, 297–308, 1984.
- [17] T.H. Green and N.J. Pearson, Ti-rich accessory phase saturation in hydrous mafic-felsic compositions at high PT, *Chem. Geol.* 54, 185–201, 1986.
- [18] R.W. Rapp, E.B. Watson and C.F. Miller, Partial melting of amphibolite/eclogite and the origin of Archean trondhjemites and tonalites, *Precamb. Res.* 51, 1–25, 1991.
- [19] I.S. McCallum and M.P. Charette, Zr and Nb partition coefficients: Implications for the genesis of Mare basalts, KREEP, and sea floor basalts, *Geochim. Cosmochim. Acta* 42, 859–869, 1978.
- [20] T.H. Green and N.J. Pearson, An experimental study of Nb and Ta partitioning between Ti-rich minerals and silicate liquids at high pressure and temperature, *Geochim. Cosmochim. Acta* 51, 55–62, 1987.
- [21] P.B. Kelemen, R.J. Kinzler, K.T.M. Johnson and A.J. Irving, High field strength element depletions in arc basalts due to mantle–magma interaction, *Nature* 345, 521–524, 1990.
- [22] P.B. Kelemen, H.J.B. Dick and J.E. Quick, Formation of harzburgite by pervasive melt-rock reaction in the upper mantle, *Nature* 358, 635–641, 1992.
- [23] H.J.B. Dick and P.B. Kelemen, Fractionation of Ti from rare earth elements during formation of harzburgite from lherzolite by magma/mantle interaction, *EOS Trans. Am. Geophys. Union* 72, 545, 1990.
- [24] E. Rampone, P. Bottazzi and L. Ottolini, Complementary Ti and Zr anomalies in orthopyroxene and clinopyroxene from mantle peridotites, *Nature* 354, 518–520, 1991.
- [25] W.F. McDonough, H.-G. Stosch and N.G. Ware, Distribution of titanium and the rare earth elements between peridotitic minerals, *Contrib. Mineral. Petrol.* 110, 321–328, 1992.
- [26] S.R. Hart and T. Dunn, Experimental Cpx/melt partitioning of 24 trace elements, *Contrib. Mineral. Petrol.* 113, 1–8, 1993.
- [27] T.H. Green, S.H. Sie, C.G. Ryan and D.R. Cousins, Proton microprobe-determined partitioning of Nb, Ta, Zr, Sr and Y between garnet, clinopyroxene and basaltic magma at high pressure and temperature, *Chem. Geol.* 74, 201–216, 1989.
- [28] J.A. Pearce and M.J. Norry, Petrogenetic implications of Ti, Zr, Y and Nb variations in volcanic rocks, *Contrib. Mineral. Petrol.* 69, 33–47, 1979.
- [29] N. Shimizu and S.R. Hart, Applications of the ion microprobe to geochemistry and cosmochemistry, *Annu. Rev. Earth Planet. Sci.* 10, 483–526, 1982.
- [30] J.F. Bender, C.H. Langmuir and G.N. Hanson, Petrogenesis of basalt glasses from the Tamayo region, East Pacific Rise, *J. Petrol.* 25, 213–254, 1984.
- [31] H.E. Newsom, W.M. White, K.P. Jochum and A.W. Hofmann, Siderophile and chalcophile element abundances in oceanic basalts, Pb isotope evolution and growth of the Earth's core, *Earth Planet. Sci. Lett.* 80, 299–313, 1980.
- [32] P.H. Nixon and F.R. Boyd, Petrogenesis of the granular and sheared ultrabasic nodule suite in kimberlites, in: *Lesotho Kimberlites*, P.H. Nixon, ed., pp. 48–56, Lesotho Nat. Dev. Corp., Lesotho, South Africa, 1973.

- [33] A.J. Erlank, F.G. Waters, C.J. Hawkesworth, S.E. Haggerty, H.L. Allsopp, R.S. Rickard and M. Menzies, Evidence for mantle metasomatism in peridotite nodules from the Kimberley Pipes, South Africa, in: *Mantle Metasomatism*, M.A. Menzies and C.J. Hawkesworth, eds., pp. 221–311, Academic Press, London, 1987.
- [34] S.H. Richardson, A.J. Erlank and S.R. Hart, Kimberlite-borne garnet peridotite xenoliths from old enriched subcontinental lithosphere, *Earth Planet. Sci. Lett.* 75, 116–128, 1985.
- [35] V.J.M. Salters, The use of Hf-isotopes and high field strength elements to constrain magmatic processes and magma sources, 267 pp., PhD Thesis, M.I.T., 1989.
- [36] G.A. McKay, Crystal/liquid partitioning of REE in basaltic systems: Extreme fractionation of REE in olivine, *Geochim. Cosmochim. Acta* 50, 69–79, 1985.
- [37] A.J. Irving and F.A. Frey, Distribution of trace elements between garnet megacrysts and host volcanic liquids of kimberlitic to rhyolitic composition, *Geochim. Cosmochim. Acta* 42, 771–787, 1978.
- [38] N. Shimizu and C.J. Allègre, Geochemistry of transition elements in garnet lherzolite nodules in kimberlites, *Contrib. Mineral. Petrol.* 67, 41–50, 1978.
- [39] T.W. Sisson and C.R. Bacon, Garnet/high silica rhyolite trace element partition coefficients measured by ion microprobe, *Geochim. Cosmochim. Acta* 56, 2133–2136, 1992.
- [40] M. Mazzucchelli, G. Rivalenti, R. Vannucci, P. Bottazzi, L. Ottolini, A.W. Hofmann, S. Sinigoi and G. Demarchi, Trace element distribution between clinopyroxene and garnet in gabbroic rocks of the deep crust: An ion microprobe study, *Geochim. Cosmochim. Acta* 56, 2371–2385, 1992.
- [41] N. Shimizu, Geochemistry of ultramafic inclusions from Salt Lake Crater, Hawaii, and from southern African kimberlites, *Phys. Chem. Earth* 9, 655–669, 1975.
- [42] H.-G. Stosch, Rare earth element partitioning between minerals from anhydrous spinel peridotite xenoliths, *Geochim. Cosmochim. Acta* 46, 793–811, 1982.
- [43] W.E. Gallahan and R.L. Nielsen, The partitioning of Sc, Y, and the rare earth elements between high-Ca pyroxene and natural mafic to intermediate lavas at 1 atmosphere, *Geochim. Cosmochim. Acta* 56, 2387–2404, 1992.
- [44] P.W. Gast, Trace element fractionation and the origin of tholeiitic and alkaline magma types, *Geochim. Cosmochim. Acta* 32, 1057–1089, 1968.
- [45] D.M. Shaw, Trace element fractionation during anatexis, *Geochim. Cosmochim. Acta* 34, 237–243, 1970.
- [46] A.E. Ringwood, The chemical composition and origin of the Earth, in: *Advances in Earth Science*, P. Hurley, ed., pp. 287–356, 1966.
- [47] J.B. Gill, Role of underthrust oceanic crust in the genesis of a Fijian calc-alkaline suite, *Contrib. Mineral. Petrol.* 43, 29–45, 1974.
- [48] I.A. Nicholls and K.L. Harris, Experimental rare earth element partition coefficients for garnet, clinopyroxene and amphibole coexisting with andesitic and basaltic liquids, *Geochim. Cosmochim. Acta* 44, 287–308, 1980.
- [49] D.J. DePaolo, Trace element and isotopic effects of combined wallrock assimilation and fractional crystallization, *Earth Planet. Sci. Lett.* 53, 189–202, 1981.
- [50] P.G. Harris, Zone refining and the origin of potassic basalts, *Geochim. Cosmochim. Acta* 12, 195–208, 1957.
- [51] D. McKenzie, The generation and compaction of partially molten rock, *J. Petrol.* 25, 713–765, 1984.
- [52] O. Navon and E. Stolper, Geochemical consequences of melt percolation: The upper mantle as a chromatographic column, *J. Geol.* 95, 285–307, 1987.
- [53] G. Vasseur, J. Vernieres and J.-L. Bodinier, Modeling of trace-element transfer between mantle melt and heterogeneous peridotite matrix, *J. Petrol. Special Lherzolites Issue*, 41–54, 1991.
- [54] P.B. Kelemen, Reaction between ultramafic wall rock and fractionating basaltic magma: Part I, Phase relations, the origin of calc-alkaline magma series, and the formation of discordant dunite, *J. Petrol.* 31, 51–98, 1990.
- [55] K.T.M. Johnson and H.J.B. Dick, Open system melting and temporal and spatial variation of peridotite and basalt at the Atlantis II Fracture Zone, *J. Geophys. Res.* 97, 9219–9241, 1992.
- [56] A.V. Sobolev and N. Shimizu, Ultra-depleted primary melt included in an olivine from the Mid-Atlantic Ridge, *Nature* 363, 151–154, 1993.
- [57] Nicolas, A., Melt extraction from mantle peridotites: Hydrofracturing and porous flow, with consequences for oceanic ridge activity, in: *Magma Transport and Storage*, M.P. Ryan, ed., pp. 159–174, Wiley, New York, 1990.
- [58] R.W. Kay, Volcanic arc magmas: implications of a melting-mixing model for element recycling in the crust–upper mantle system, *J. Geol.* 88, 497–522, 1980.
- [59] J.H. Davies and D.J. Stevenson, Physical model of source region of subduction zone volcanics, *J. Geophys. Res.* 97, 2037–2070, 1992.
- [60] J.A. Grow, Crustal and upper mantle structure of the central Aleutian arc, *Geol. Soc. Am. Bull.* 84, 2169–2192, 1973.
- [61] G.C. Brown, Mantle origin of Cordilleran granites, *Nature* 265, 21–24, 1977.
- [62] A.E. Ringwood, The petrological evolution of island arc systems, *J. Geol. Soc. London* 130, 183–204, 1974.
- [63] R.W. Kay, Aleutian magnesian andesites: Melts from subducted Pacific ocean crust, *J. Volcanol. Geotherm. Res.* 4, 117–132, 1978.
- [64] S.M. Peacock, Numerical simulation of subduction zone pressure–temperature–time paths: constraints on fluid production and arc magmatism, *Philos. Trans. R. Soc. London A* 335, 341–353, 1991.
- [65] N. von Bargen and H.S. Waff, Wetting of enstatite by basaltic melt at 1350°C and 1.0- to 2.5-GPa pressure, *J. Geophys. Res.* 93, 1153–1158, 1988.

- [66] H. Martin, Effect of steeper Archean geothermal gradient on geochemistry of subduction-zone magmas, *Geology* 14, 753–756, 1986.
- [67] T. Plank and C.H. Langmuir, Sediments melt and basaltic crust dehydrates at subduction zones, *EOS Trans. Am. Geophys. Union* 73, 637, 1992.
- [68] M.R. Carroll and P.J. Wyllie, Experimental phase relations in the system tonalite–peridotite–H<sub>2</sub>O at 15 kb: Implications for assimilation and differentiation processes near the crust–mantle boundary, *J. Petrol.* 30, 1351–1382, 1989.
- [69] E. Anders and N. Grevesse, Abundances of the elements: Meteoritic and solar, *Geochim. Cosmochim. Acta* 53, 197–214, 1989.
- [70] R.J. Kinzler and T.L. Grove, Primary magmas of mid-ocean ridge basalts 2. Applications, *J. Geophys. Res.* 97, 6907–6926, 1992.
- [71] C.J. Allègre, S.R. Hart and J.-F. Minster, Chemical structure and evolution of the mantle and continents determined by inversion of Nd and Sr isotopic data, II: Numerical experiments and discussion, *Earth Planet. Sci. Lett.* 66, 191–213, 1983.